THE JOURNAL OF PHYSICAL CHEMISTRY C

ARTICLE

pubs.acs.org/JPCC

Microscale Spatially Resolved Thermal Response of Si Nanotip to Laser Irradiation

Xiangwen Chen and Xinwei Wang*

Department of Mechanical Engineering, 2010 Black Engineering Building, Iowa State University, Ames, Iowa 50011, United States

ABSTRACT: Under laser irradiation, the atomic force microscope (AFM) tip can give rise to strong near-field scattering and focusing, leading to strong heating of the tip itself. We report a systematic study of laser heating of an ordinary AFM silicon tip under lateral laser irradiation with micrometer spatial resolution. The temperature rise of the tip can be determined from the relationship between Raman shift versus temperature. The influences of focal situation and energy density of the incident laser on the Raman shift/temperature are studied extensively. The microscale spatially resolved temperature response is also investigated when the laser spot moves along the tip axis until to the cantilever. When the laser irradiates the tip apex, the middle of the tip, and the cantilever, the corresponding temperatures are 603, 754, and 626 K under laser density of 5.6×10^8 W/m^2. We substantiate our Raman measurement by theoretically modeling the electric field distribution using the finite element method as well as the heating processing by a one-dimensional heat transport model. Sound agreement between the modeling and experimental result is observed, and discussions are provided about the reasons for their discrepancy.

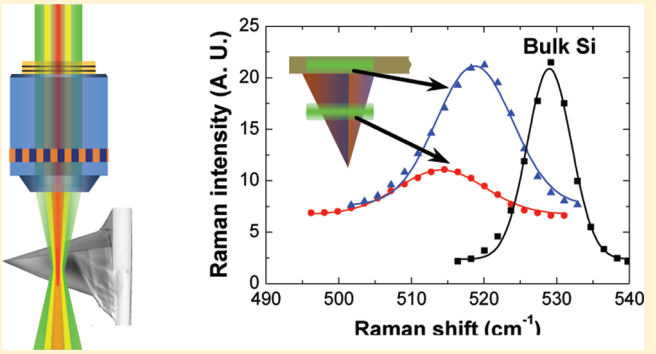

1. INTRODUCTION

When an external laser illuminates a nanoscale tip, heating effect arises from absorption of light. This thermal phenomenon happens in near-field scanning optical microscopy (NSOM),[1−5] apertureless NSOM,[6,7] tip-enhanced Raman spectroscopy (TERS),[8] laser-assisted scanning tunneling microscope (STM)/atomic force microscope (AFM)-assisted surface modification and nanofabrication,[9−11] and high density data storage.[12−14] In aperture NSOM, during the process of passing light through the aperture, a large portion of the incident laser is trapped in the tip area, causing tip heating.[1,2] As heat accumulated near the tip apex, the probe could be damaged as a result of thermal stress caused by different thermal expansions of the fiber and aluminum coating of the coaxial tip.[3−5] For an apertureless tip, a very strong electromagnetic field is created in the vicinity of the tip apex, which may cause nanoscale heating effects in the tip.[6,7] Mamin and Rugar first used a laser-heated AFM tip and cantilever to create a series of 100 nm depth pits on polymer substrates.[12] Hamann et al. used a laser-heated AFM tip magnetic recording method, which is beyond traditional limits, to heat a magnetic material and write less than 40 nm pits, corresponding to a data density of 400 Gbit/inch^2.[14] The heated tip can be used as a sharp, nanoscale knife.[15−17] Tarun et al. cut CNTs using a heated silicon tip whose temperature is as high as 1400 K as a nanoscale heat source.[17] Heat flow between the contacted tip and substrate was also investigated[18,19] in the past.

In tip-based experiments, the tip heating is important for controlling the results, the depth and width of nanoscale pits in nanosurface modification. Even in TERS, the heated then thermal expanded tip will affect the results. An annealing effect triggered by a local temperature rise of 20−30 K in the substrate would make the Au surface smoother and cause irreversible Raman signal loss.[8] Usually, the heating needs to be controlled to ensure the tip does not adversely affect the sample, especially in probing biological and polymetric materials.

In fact, all of the technologies introduced above did not measure the exact temperature. The only control approach is to tune the input laser intensity to control the temperature of the tip in a reasonable range, which in turn determines the thermal expansion for specific materials. Specifically, the temperature models[10,11,20,21] as well as thermal expansion[10,15,21−25] for the thermal tips have been reported extensively. Thermal expansion of tips was usually measured under STM mode, for the tip−substrate distance is readily calculated through tunneling current−gap relationship.[25] Also, theoretical calculation of the temperature rise[26] or temperature distribution[6−9,20] provides powerful inspection for laser heated tips.

Experimental work for measuring the temperature of heated tips due to laser absorption was mainly done through Raman spectroscopy.[9,13,17] The resonance frequency shift method was introduced to investigate the temperature of both AFM tip and cantilever under lateral laser illumination.[9] The latter one,

Received: July 25, 2011
Revised: October 5, 2011
Published: October 06, 2011

Table 1. Some Experimental Determinations about Temperature-Dependent Raman Spectra of Si

researcher	temperature range (K)	Si morphology	slope (cm^{-1}/K)
Yue et al.[27]	300−503	bulk	−0.022
Hubert et al.[60]	295−900	bulk	−0.0247
Doerk et al.[41]	293−593	bulk	−0.022
		nanowire	
Khachadorian et al.[34]	272−700	bulk	−0.0229
	272−873	nanowire	−0.0236

although less accurate, is amenable for practically all standard AFMs.

In our previous work, the thermal response of tungsten AFM tips under laser irradiation was systematically investigated.[7] Furthermore, more than 200 °C at sub-10 nm scale on silicon substrate under laser illuminated tip was also observed in experiment.[27] In this work, Raman thermometry is used to investigate the temperature rise of silicon AFM tip induced by the near-field laser heating. Raman thermometry as a noncontact temperature measurement method is extensively used for studying thermal transport in micro/nano structures, like CNTs,[28,29] molecular junctions,[30] GaAs nanowires,[31] silicon nanowires,[32−35] and nanogranular silicon.[36] In Raman thermometry, as the temperature increases, the width broadens, and the peak position shifts toward lower frequency.[33,37,38] Both characteristics have been used to determine local temperature. The temperature can also be determined by the Stokes/anti-Stokes intensity ratio, which depends on temperature through the Bose−Einstein occupation number $I_{\text{anti-Stokes}}/I_{\text{Stokes}} \propto \exp(-\hbar\omega/k_B T)$,[13,17,30,36,37,39] if both of the Stokes and anti-Stokes peaks are available. Selection of these methods has been discussed elsewhere.[27] The material used in our experiment is Si, which can provide sharp peak signal. However, the intensity of the Raman signal is relatively low when only a small portion of the tip apex stays in the laser beam. As a result, the Raman shift method is chosen in the experiments.

The temperature-dependent Raman shift for silicon material (including bulk material, nanowires, and nanoparticles) has been studied thoroughly in the last 40 years.[34,36,37,39−41] Balkanski et al.[39] presented a theoretical model of Raman frequency versus measured temperature from 5 to 1400 K, using three- and four-phonon processes. It can be inferred that linear regress is closely satisfied from room temperature to 600 K.

Table 1 shows the linear relationship between the Raman shift and temperature for both bulk silicon and silicon nanowires reported by many groups. Although the relationships between the temperature and Raman shift for bulk Si and Si nanowire are the same[41] or of little discrepancies,[34] the dependence of Raman shift on temperature for AFM Si tip is highly different. McCarthy et al.[13] observed a red-shift between the Raman shift from bulk Si and Si tip, due to the geometry of the sharp tip. Tarun et al.[17] also reported a Raman shift versus temperature curve for lateral laser heating Si tips, and the data are a little larger than those obtained by McCarthy et al.[13]

In laser-assisted tip-based experiments, the highly focused laser beam size, usually as small as several micrometers,[9] is comparable to the size of the tips, so focusing is of great importance. It is hard to control the interaction between the laser and tip during experimental work. To our best knowledge, few experimental investigations have been reported on how the extremely focused laser beam irradiates different spots of the relatively long AFM tip, while such work can provide guidance for high-degree experimental control. In this work, microscale spatially resolved experimental examination is done to explore how the thermal response changes when the laser illuminates the different spot of the tip with different laser power.

2. EXPERIMENTAL SETUP

Figure 1a sketches the schematic of the experimental setup. The experimental Raman microscope system consists of a confocal Raman spectrometer (Voyage, B&W Tek, Inc.) and microscope (Olympus BX51). The spectral resolution of the Raman system is 1−2 cm^{-1}. An ordinary AFM silicon tip, which is mounted on a three-dimensional piezo-actuated nanostage is located under the focal spot of the laser beam from the Raman spectrometer. The tip axis is horizontal and along the y direction of the nanostage. The cantilever is along the x direction, and the laser is incident vertically along the z direction. The movement range of the nanostage is 20 μm (using combination with a second one-dimensional piezo-actuated nanostage, the range in the y direction is 40 μm), with a resolution of 20 nm in each direction. The whole system is placed in air.

The laser beam is focused through a 20× microscope objective (NA = 0.40, WD = 12.0 mm). The beam size is 2.8 × 10.0 μm^2 at the focal spot as shown in Figure 1b. The laser beam is partially polarized along the x' and y' directions as shown in Figure 1b. The nanostage is aligned to make sure that the laser is incident from the z direction. The tip axis is perpendicular to the longer side of the laser spot. In such case, the tip axis has an angle of 45° with respect to the direction in which the polarized laser has the strongest intensity.

The laser with wavelength of 532 nm is used as both Raman probe and heat source. The optical trace is also shown in Figure 1. The incident laser from the Raman spectrometer is focused on the tip under the objective lens. The excited Raman scattering signal and Rayleigh scattering signal are collected by the same objective in the backscattering mode: it sends the scattered radiation backward to the spectrometer. To investigate the heating effect caused by laser, the tip is illuminated with different laser power of 4, 7, 12,7 and 15.9 mW, corresponding to energy fluxes of 5.6 × 10^8, 4.5 × 10^8, 2.5 × 10^8, and 6 × 10^8 W/m^2, respectively, at the focal spot. All Raman spectra are measured using an integration time of 10 s, unless otherwise stated.

Single crystal silicon (antimony doped) tip (CSG10, K-Tek nanotechnology) is used in the experiment. Figure 2 shows the SEM image of the AFM tip. It clearly shows that the shape of tip is tetragonal pyramid. The thickness of the cantilever is 2.67 μm, and the length of the tip is 15.37 μm. The front plane angle is 10°, the back plane is 30°, and side angle is 36°. The last 500 nm from tip apex is conical with a cone angle of 10°. The apex radius is 10 nm. According to the dimensions of the tip, the laser width can only partially cover the tip, as shown in Figure 1b. To keep consistence, all of the data in the following figures are measured on the same tip.

3. EXPERIMENTAL RESULTS AND DISCUSSION

3.1. Temperature Determination Based on Shift of Raman Peak. To analyze the thermal response of the tip under laser

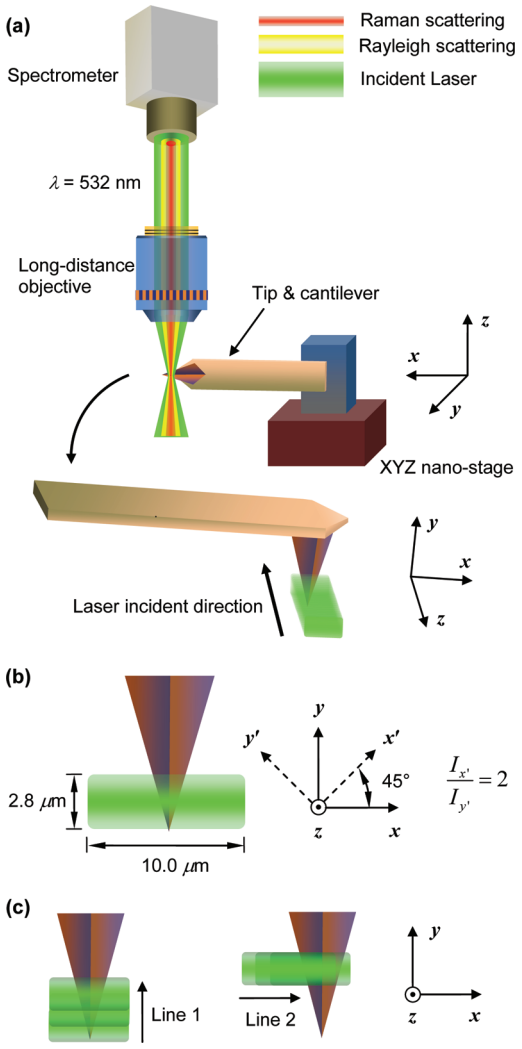

Figure 1. (a) Schematic of experimental setup (not to scale). An ordinary AFM silicon tip that is set on a three-dimensional piezo-actuated nanostage is located under the focal spot of the laser beam from a Raman spectrometer. The tip axis is horizontal and along the y direction. The cantilever is along the x direction. The laser is incident vertically from the z direction. The movement range of the nanostage is 20 μm, with resolution of 20 nm. (b) Configuration of the laser beam at the focal spot when the laser illuminates the side surface of tip. The spot size of the incident laser is 10.0 μm along the x direction, and 2.8 μm along the y direction. The laser beam is polarized with the strongest intensity along the x'-axis twice that along the y'-axis, where the x'- or y'-axis has a 45° angle with respect to the major axis or minor axis. (c) Laser spot moving directions with respect to the tip during experiment. Actually, during the experiment, the laser beam is fixed, and the tip moves relative to the laser beam controlled by the 3-D nanostage. To straightforwardly explain the relative movement between the laser and the tip, for some cases, the tip is considered fixed, and the laser beam is considered movable.

illumination by using the Raman shift method, the temperature dependence of the Raman shift of Si tip is needed. Although plenty of results of the relationship between the temperature and Raman shift have been reported for bulk Si as well as Si nanowires introduced above, these results would not be suitable for the Si tip due to discrepant geometries. Balkanski et al.[39] gave a theoretical calculation equation of the peak position $\omega(T)$ versus

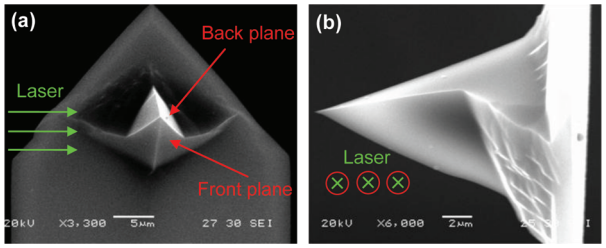

Figure 2. (a) Top-view and (b) side-view SEM images of the AFM tetragonal pyramid tip. The thickness of the cantilever is 2.67 μm, and the length of the tip is 15.37 μm. The front plane angle is 10°, the back plane is 30°, and the side angle is 36° (the front/back plane angle is the angle of projection of the front/back plane from side-view, and the side plane angle is the angle of the projection of front/back plane from front/back-view). According to the data provided by the supplier of the tip, the last 500 nm from tip apex is conical with a cone angle of 10°, and the apex radius is 10 nm.

temperature for bulk Si as

$$\omega(T) = \omega_0 + C\left(1 + \frac{2}{e^x - 1}\right) + D\left(1 + \frac{3}{e^y - 1} + \frac{3}{(e^y - 1)^2}\right) \quad (1)$$

where ω_0 is Raman frequency at 0 K with a value of 528 cm^{-1}, and C and D are anharmonic constants corresponding to three- and four-phonon processes with the values of −2.96 and −0.174 cm^{-1}, respectively. $x = \hbar\omega_0/2k_BT$, and $y = \hbar\omega_0/3k_BT$, where $\hbar$ is the reduced Planck's constant, and k_B is the Boltzmann constant. To make it suitable for AFM tip, McCarthy et al.[13] revised this anharmonic model by doubling of four-phonon nonlinear effects (i.e., D = −0.348 cm^{-1}) and proved it fits the relationship between Raman shift and temperature of laser-heated Si AFM tips. The temperature was measured from anti-Stokes/Stokes. Tarun et al.[17] also measured the Raman shift and temperature of Si tip heated by lateral incident laser and found the result can be approximately fitted by the model used by McCarthy et al.,[13] although the experimental results are a little higher. The curves for both theoretical models are shown in Figure 3. To make these curves suitable for the experiments data here, the initial values of the theoretical models are reset as compared to the original ones due to system shift, that is, ω_0 = 535 cm^{-1}. This value is determined by making the curve calculated by Balkanski et al.[39] go through the point (298 K, 529.05 cm^{-1}), measured on bulk Si at room temperature. Once the initial value of the model describing bulk Si is set, it is also the same for the model describing Si tips. For comparison, the linear fitting between temperature and Raman shift for bulk silicon with a slope of −0.022 cm^{-1}/K is also shown in Figure 3. It indicates that the line for the linear relationship from room temperature through 700 K for bulk Si is almost overlapped with that of the Balkanski's anharmonic model.

The temperature rises of the AFM tip are measured by the Raman shift, and the temperature is obtained through the theoretical calculation introduced by McCarthy et al.[13] The results are fully reproducible, over five replications of each measurement were performed, and one representative result (curve) is chosen for each, as presented in Figures 4−7. From Figure 5 to 7, the temperature axis is calibrated according to the relationship between the Raman shift and temperature in Figure 3, and, as a result, it is not linear. The shape of each curve

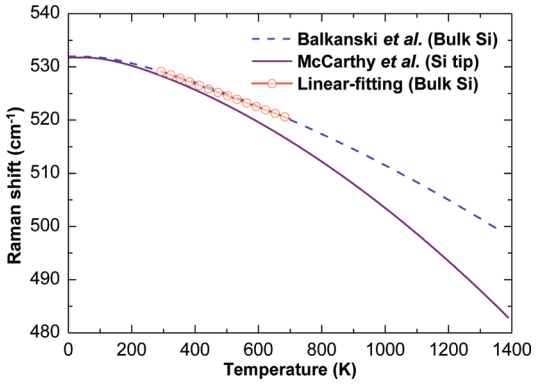

Figure 3. Temperature dependence of the Raman shift for bulk Si (dashed line and red circles) and Si AFM tip (solid line), obtained from the calculations of Balkanski[39] and McCarthy,[13] and linear fitting with a slope of −0.022 cm^{-1}/K. The dashed curve represents the model using both three- and four-phonon processes. The solid curve is revised on the basis of Balkansik's model by doubling of four-phonon nonlinear effects, making it suitable for tip geometry. To make curves suitable for the experiments data here, the initial values of the theoretical models are reset as compared to the original ones.

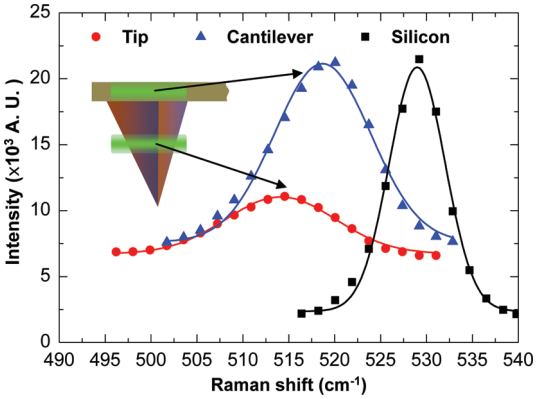

Figure 4. Raman shift when the laser illuminates the side surface of tip, side surface of cantilever, and bulk silicon, respectively. To keep the intensity of the spectrum for Si substrate comparable to others, a 5 s integration time is used, as compared to 10 s in the Raman measurement.

reported in this work is reproducible. However, the curve drifted a little bit in terms of absolute value from experiment to experiment. The drifts could be induced by the systematic error of the Raman spectrometer and the deviation of the relative position of the tip with respect to the laser beam. The latter, after all, is monitored by eyes through optical image of the tip under the objective lens. The drift induced by the Raman system is suppressed to the minimal level by observing the Raman spectrum when the laser irradiates the center of the side surface of the tip as shown in Figure 4. The repeatability of the curve is controlled to be better than 0.5 cm^{-1} from experiment to experiment. Still, we feel that the difference between experiment and experiment is largely due to the heating position difference of the tip, and not the measurement itself.

In analysis of Raman spectrum, due to the resolution limit of the Raman spectrometer, the peak position is determined by Gaussian function fitting, which is consistent with our calibration.[27] With the Gaussian fitting, the Raman spectral

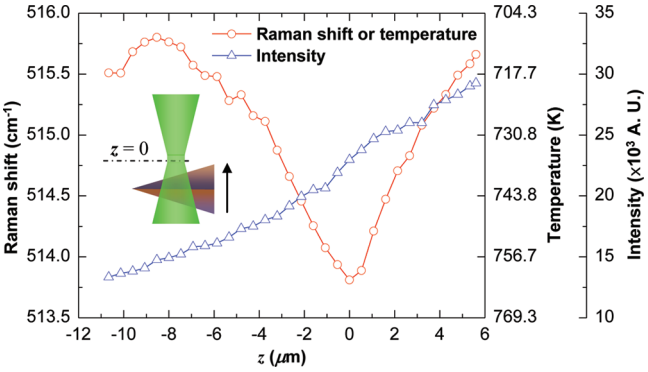

Figure 5. Raman shift, temperature, and Raman intensity when the tip moves upward along the z direction in the vicinity of focal spot.

resolution can be improved from 1−2 to 0.05 cm^{-1}. Figure 4 shows selected spectra for situations that the laser beam laterally irradiates AFM tip and cantilever (as shown in Figure 2b), and vertically irradiates on bulk Si, respectively. To keep the height of the spectrum for the Si substrate comparable to others, 5 s of integration time is used, as compared to 10 s in the Raman measurement. The Raman shifts are 514.20, 518.70, and 529.05 cm^{-1}, respectively, for the three peaks. We attribute the peak position change of the spectrum to laser heating. The corresponding temperature of the Si substrate is considered as room temperature, 298 K. The temperatures of the tip and cantilever are 754 and 626 K, respectively. Another phenomenon is that the width of the Raman peak will change as temperature changes, usually broadens as temperature increases. This is also caused by the heating effect. As a result, this characteristic can also be used to determine the temperature of the tip.[42,43] However, due to the weak Raman signal when only a small portion of the tip apex is under laser irradiation, it is not straightforward to measure the line width [full width at half-maximum (fwhm)] of the peak. Therefore, this method is not used in this Article. The broadening of the peak will not affect the precision of peak position determination with the aid of Gaussian fitting adapted here.

3.2. Microscale Spatially Resolved Temperature Response. In our experiment, the focusing has a significant effect on the experimental results, as the dimension of the laser beam at the focal spot and that of the tip are comparable. The size of the laser beam in the x direction is 10.0 μm, and it can cover the tip in the x direction, even at the position where the tip connects to the cantilever (where the projectable width is 12.4 μm according to the SEM observation in Figure 2b). All of the temperatures measured in this work are volumetric averaged values, for the Raman signal for temperature determination comes from the volume under laser irradiation. If the size of the laser beam in the x direction is smaller, say 3−5 μm, it would be hard to determine the relative position of the laser beam to the tip in the x direction. Although reducing the size of the laser beam in the y direction could get a higher spatially temperature resolution in the y direction, the decrease in heating area would bring the tip to another state of thermal equilibrium.

In Figure 5, the laser beam illuminates the center of the lateral surface of the tip, as shown in the joint point of lines 1 and 2 in Figure 1c. The three-dimensional nanostage is adjusted along the z-axis to change the position of the tip around the focal spot. The total travel distance is about 17 μm, covering the focal spot

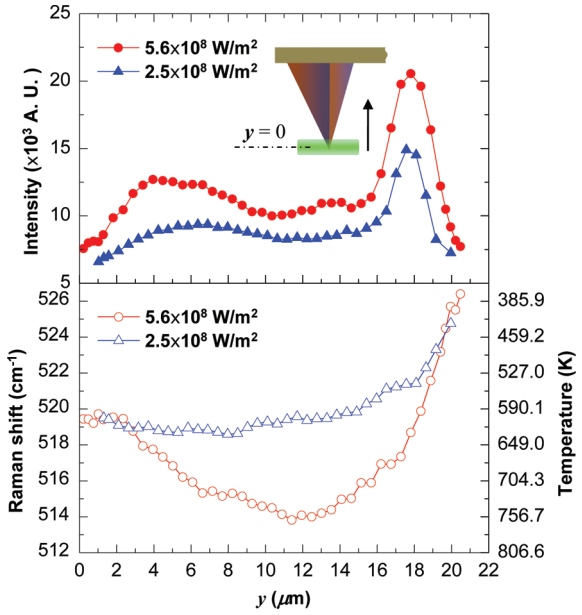

Figure 6. Raman intensity and Raman shift along line 1 [as shown in Figure 1c, in y direction] under energy fluxes of 5.6×10^8 and 2.5×10^8 W/m^2, respectively. The laser spot moves along the tip axis. When $y = 0$ μm, 1.6 μm in width of the laser has entered into the region of the tip (the width of the beam at the focal spot is 2.8 μm), as the schematic diagram of tip and laser shows.

($z = 0$ μm). The focusing situation is monitored by the diffraction image under the tip, to ensure a reliable and reproducible focusing alignment. When the tip moves upward (below the focal spot) approaching the focal spot, an image following the same orientation of the tip can be observed under the tip. The image zooms out as the tip moves upward. When the tip is within the range of ± 2 μm of the focal spot, the image disappears because the laser beam is completely blocked by the tip. As the tip moves upward further, the image orientation is reversed.

During the travel of the tip, when the tip is over 8.5 μm lower than the focal spot ($z < -8.5$ μm), the Raman shift increases as the tip approaches the focal spot; correspondingly, the temperature decreases. In this process, the further the tip is away from the focal point, the larger area of the tip is covered by the laser beam. Consequently, more energy is absorbed by the tip, which in turn results in higher temperature rise. When the tip is less than 8.5 μm below the focal spot (-8.5 μm $< z < 0$ μm), the Raman shift decreases (temperature increases) as the tip is closer to the focal spot. When the tip gets over the focal spot ($z > 0$ μm), the Raman shift increases (temperature decreases) as the tip is away from the focal spot. When $z > -8.5$ μm, the closer the tip is to the focal spot, the higher energy density the incident laser has. As a result, the tip reaches a higher temperature. How the energy density affects the temperature rise of the tip will be discussed later. When the tip goes up and approaches the objective lens, the Raman intensity increases due to the increase of the collection angle.

As the illuminating laser beam moves along the tip axis (parallel to line 1 in Figure 1c) from the tip apex to the cantilever, the Raman signal intensity and Raman shift (temperature) are shown in Figure 6. In this process, the Raman signal is integrated along the y axis with a size of 2.8 μm. First, the situation for incident laser of 5.6×10^8 W/m^2 is considered. When the laser spot begins to be in contact with the tip apex, Raman signal

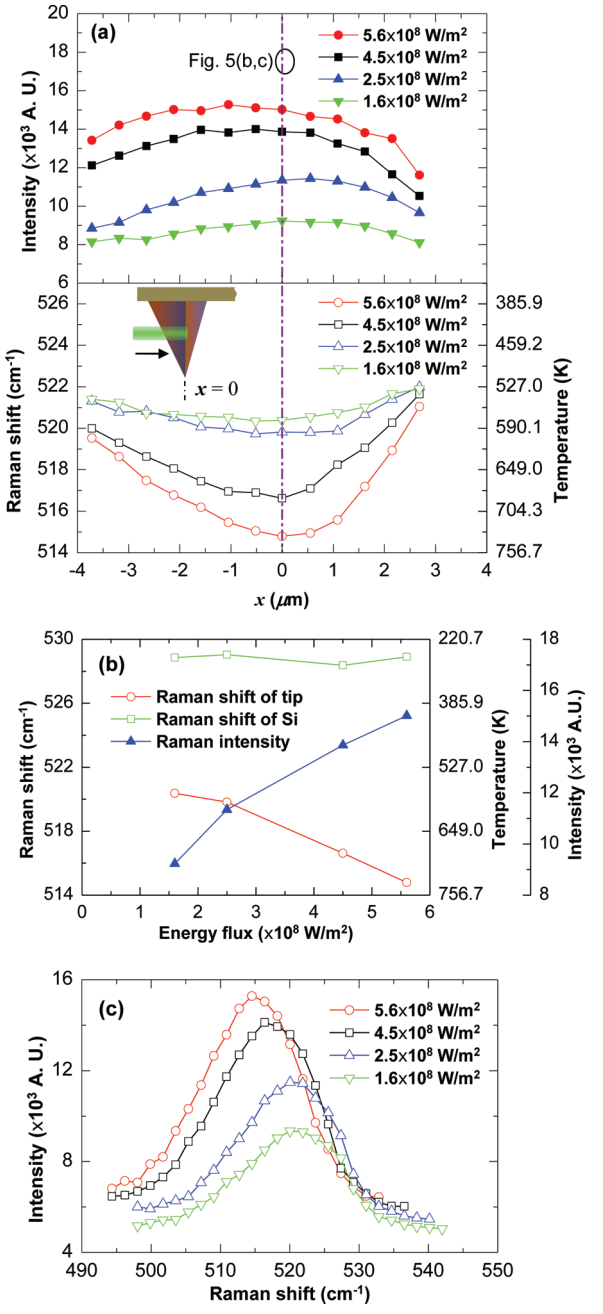

Figure 7. (a) Raman intensity and Raman shift along line 2 [as shown in Figure 1c, in the x direction] under energy fluxes of 5.6×10^8, 4.5×10^8, 2.5×10^8, and 1.6×10^8 W/m^2, respectively. The tip is at the focal spot level of the laser beam. The laser spot moves perpendicularly to the tip axis. The signal is collected when half of the laser beam has covered the tip as the schematic of the tip and laser shows. (b) Raman shift and Raman intensity versus energy flux. The Raman shift of bulk silicon is also shown in the figure (green □). (c) Raman peak under different energy fluxes. In (b) and (c), the laser spot is symmetrical about the tip axis ($x = 0$ μm).

emerges. However, only a small part of the laser illuminates the tip, the Raman signal intensity is very low, and the Raman shift is too weak for proper fitting to find the peak position. When the tip entered into the laser beam for about 1.6 μm, at $y = 0$ μm in Figure 6, an obvious Raman peak is observed. The Raman shift is approximately 519.5 cm^{-1}, and the temperature is 603 K, as

dx.doi.org/10.1021/jp2070979 |J. Phys. Chem. C 2011, 115, 22207–22216

depicted by red open circles. Because the width of the laser spot along the tip axis is 2.8 μm, it can be conclusive that over one-half of the laser beam irradiates the tip apex and generates the obvious Raman peak signal.

As the laser moves further toward the base of the tip, that is, from $y = 0$ μm to $y \approx 15.5$ μm, the Raman shift decreases gradually from 519.5 to 514.0 cm^{-1} when 0 μm $< y <$ 11.5 μm, and increases to 515.0 cm^{-1} when 11.5 μm $< y <$ 14 μm, indicating the temperature increases from 603 to 754 K, then declines to 728 K. This is the trade-off between the increasing of laser absorbing area and the increasing heat conduction to the base of the tip even the cantilever. When the laser beam scans along the tip axis, the area of the tip under laser illumination will increase, and more electromagnetic energy is absorbed to convert into heat. On the other hand, the closer the laser is to base of the tip, the easier the heat is conducted away into the cantilever, which can be considered a heat sink. Meanwhile, as the laser is away from the tip apex, the field enhancement effect becomes weaker, and the laser intensity around the tip, which in turn will decide the laser absorption inside silicon tip, will inevitably decline.

The curve of Raman signal intensity is affected by both the size of the laser−tip interaction area and the heating situation. As the area of the laser illumination increases, the Raman signal intensity increases, as shown for $y <$ 4 μm in Figure 6. On the other hand, when 4 μm $< y <$ 10.5 μm, the Raman signal intensity decreased so obviously. When temperature increases, the state density of phonons will increase; consequently, the phonons will have a higher energy. This will induce a reduction of intensity of Stokes scattering.[33] The intensity of Stokes Raman peak is proportional to $n(\omega) + 1$, where $n(\omega) = [\exp(-\hbar\omega/k_BT) - 1]^{-1}$ is the Bose−Einstein distribution function, or the thermal occupation number.[44] Under this condition, the intensity of the Stokes Raman scattering drops when the temperature rises. This effect has also been observed in silicon substrates under illuminated AFM tip in our previous work[27] and in silicon nanowires.[33] For 10.5 μm $< y <$ 14 μm, under the combined effects of decreasing field enhancement effect, increasing illumination area, and increasing heat conduction, the Raman intensity keeps increasing slowly.

When $y >$ 14 μm, the laser beam starts to irradiate the cantilever. The arch of the curve for the Raman intensity in Figure 6 can clearly show interaction between laser and the cantilever. Figure 6 shows that the peak width of the Raman intensity curve around $y = 18$ μm is about 5.5 μm. The thickness of the cantilever is 2.67 μm, and the dimension of the laser is 2.8 μm. From the position that the laser spot starts to irradiate the cantilever until it completely moves away from the cantilever, the distance the laser focal spot travels is 5.47 μm, agreeing well with the peak width observed in Figure 6. On the left side of the peak position (14 $< y <$ 17.75 μm), the laser is still partially in contact with base of the tip. Because of the fact that the intensity signal from the tip is much lower than that from the cantilever, the signal partially from the tip does not affect the symmetry of the intensity signal. The story is different for the Raman shift. While the laser beam goes across over the side face of the cantilever, the Raman shift increases.

When the energy flux takes 2.5×10^8 W/m^2, the trend of the curve for Raman intensity is the same as but stays consistently below that under an energy flux of 5.6×10^8 W/m^2. Also, the Raman shift stays consistently higher or temperature stays consistently lower for low energy flux, except when the laser irradiates the tip apex and the cantilever as shown on both ends of the curves in Figure 6, where the Raman shift is not sensitive to the energy flux. When the laser irradiates the foremost end of the tip ($y <$ 3 μm), only a small area of the tip is exposed to the laser beam. The heat in the tip apex is readily transported to the blunt end of the tip. Although the energy flux increases from 2.5×10^8 to 5.6×10^8 W/m^2, the temperature remains at approximately 600 K. When the laser irradiates the cantilever, the heat is mainly dissipated along the cantilever to the chip, as increasing the energy fluxes does raise the temperature of the cantilever when the laser is just on the center of the cantilever ($y \approx 17.75$ μm); the Raman shift is smaller and the temperature is higher for higher energy flux. However, when the laser irradiates the edge of the cantilever (opposite side of the tip apex), only a small area of the cantilever is covered by the laser, and, as a result, the absorbed heat is transferred quickly, and the Raman shift or temperature is much less sensitive to energy flux. This phenomenon is similar to the situation when the laser irradiates bulk Si, which will be analyzed in the following discussions. Overall, the change of the Raman shift/temperature is mild for low energy flux. It experiences an almost plateau for $y <$ 8.5 μm and increases/decreases gradually for $y >$ 8.5 μm.

To investigate the local heating effect by laser irradiation, Raman scattering was performed with different laser power. Figure 7 shows the Raman signal, Raman shift, and temperature when the laser beam scans perpendicularly to the tip axis across the middle of the tip (line 2 as shown in Figure 1c) under energy fluxes of 5.6×10^8, 4.5×10^8, 2.5×10^8, and 1.6×10^8 W/m^2, respectively. The width of the tip along line 2 is approximately 7 μm. To ensure high-quality signal, the data for the laser beam irradiating the edge of the tip are neglected.

The Raman signal intensity and Raman shift/temperature are shown in Figure 7a. As expected, the Raman intensity is stronger for higher energy fluxes, and the intensity is stronger in the center as compared to that on both sides, even though not clearly sensitive to the position in the x direction. Figure 7a also indicates that higher energy flux gives rise to lower Raman shift signal and induces higher temperature rise. For each curve corresponding to a certain energy flux, when the laser moves away from the center to either side, the Raman shift/frequency increases, and the temperature of the tip drops. To investigate the influence of the energy fluxes on the signals when the laser illuminates the same spot under different energy fluxes, the signals from the center spot of the lateral surface on the tip (the joint point of lines 1 and 2 in Figure 1c, corresponding to $x = 0$ μm in Figure 7a) are presented, as shown in Figure 7b. The Raman signal intensity increases as the energy flux goes up. As expected, when the energy flux of the incident laser increases, more energy will be absorbed, the temperature of the tip also increases, which is also reflected by the decreasing Raman shift as depicted by the red open circles. The same trend for Raman shift was also observed on AFM tips,[9,13] silicon nanowires,[32,35] and nanogranular silicon films.[36] The Raman shift of bulk silicon is also shown for comparison in Figure 7b (green □). The energy fluxes in the range of $(1.6-5.6) \times 10^8$ W/m^2 on the tip have significantly modified the Raman spectra of the tip; however, it has no effect on bulk silicon, as even the density is as high as 4×10^9 W/m^2 [32] or 13.73×10^9 W/m^2 as reported in the literature.[35] The decrease of Raman shift, or temperature rise as the input energy increases, is attributed to low thermal conductivity of silicon in nanostructure[18] and the small scattering volume, as the cantilever is the only effectively way for the heat to be transferred away. For

bulk silicon, the heat generated due to laser absorption is quickly dissipated in three dimensions. However, it is worth mentioning that when the input energy is rather low, say 3×10^4 W/m^2, the situation would be different: the increasing power of incident laser has no significant effect on the Raman shift when the laser is incident on silicon nanowires.[33] Because of the low quality of the Raman peak under low energy fluxes, say $<1.6 \times 10^8$ W/m^2, no experimental data are available within this energy fluxes range for AFM Si tips.

The Raman spectra corresponding to Figure 7b are shown in Figure 7c. Obviously, the Raman shift/frequency decreases, the temperature increases, and the Raman signal intensity increases as the energy flux goes up. It has been analyzed in Figure 6 that the rising temperature/decreasing of Raman shift will reduce the Raman scattering intensity. Thus, it can be inferred that the increasing intensity due to the increasing energy flux has already been partially offset by the effect induced by rising temperature.

4. THEORETICAL ANALYSIS

4.1. Electrical Field Around and Inside the Si Tip. To analyze the mechanism of temperature rise in the silicon tip, numerical calculation of the electromagnetic field enhancement is conducted. The phenomenon of electromagnetic field enhancement around a sharp tip has been theoretically studied over years. In this work, the finite element method (FEM),[7,45−51] which has its merits in solving complex geometries, is employed to calculate the electric field distribution around as well as inside the tip.

The modeling is performed by using High Frequency Structure Simulator (HFSS V13, Ansys, Inc.), a full-wave high-frequency 3D finite element modeler of Maxwell's equations. A conical Si tip whose sharp end is tangent to a hemisphere is investigated in this work. Although the geometry of the tip used in the experiment is tetragonal pyramid, at least the last 500 nm from the apex is conical. Therefore, the conical tip model (length L = 600 nm, cone angle θ = 10°, apex radius r = 10 nm) is adopted. Maxwell's equations are solved across a defined rectangular computational domain with dimensions of 750 nm × 750 nm × 850 nm, containing the tip and vacuum around the tip. Absorbing (radiation) boundaries that balloon the boundaries infinitely far away from the structure are applied for the domain. A plane wave polarized along the tip apex is incident horizontally (perpendicular to the tip axis), and the electric field amplitude of the wave is set to 1 V/m. More details about the simulation can be found elsewhere.[7]

Figure 8 shows how the electric field is distributed around/inside the tip. It is obvious that the electric field is enhanced and confined around the tip. The strongest electric field with a magnitude of 5.19 V/m appears just under the apex. For the electric field inside the tip, due to high absorption of laser for Si, the maximum field enhancement is as high as 2.14, higher than that in tungsten tip, which is about 1 according to our previous simulation.[7] In Figure 8b, it clearly illustrates that the electric field in the center is stronger than that close to the surface, in contrast to the field distribution inside the tungsten tip, in which the electric field decays exponentially when transmits into the center of the tip.[7] For metal, the skin depth is relatively shorter than dielectric materials. For example, the skin depths of tungsten and silicon at λ = 532 nm are δ_w = 31.1 nm ($\delta = \lambda/2\pi\kappa$, κ is the extinction coefficient) and δ_{Si} = 1.64 μm, respectively. For the tungsten tip, the skin depth is far less than the dimension of the tip except at the apex. Consequently, the laser is only absorbed near the surface of the tip, and attenuation near the surface is observed. Adversely, the skin depth of Si is much larger than the width of the tip, and the laser has penetrated through the tip. Moreover, the laser in the Si tip will be reflected back and forth inside the tip when it encounters the surface. The light is trapped in the geometry as in Al-coated fiber for aperture NSOM.[1,2] In the apex, although the electric field is high enough outside, the electric field inside is relatively low. Near the apex zone, the surface of the tip exposed to the incident laser is smaller than that of the blunt zone. As a result, the total absorbed laser energy is relatively less in this zone. This explains why the strongest electric field inside the tip is not at the apex.

4.2. Temperature Rise of the Tip. With the knowledge of the electric field distribution inside the tip, the heat generation rate per unit volume can be calculated from $\dot{q} = I\beta$, where I is the laser intensity inside the tip, and β is the absorption coefficient, which is related to the extinction coefficient, κ, by $\beta = 4\pi\kappa/\lambda$. The laser intensity inside the tip equals the Poynting vector, $I = P = 0.5c\varepsilon_0 nE^2$. Here, E is the time-average intensity of the electric field, c is the light speed in free space as 3×10^8 m/s, ε_0 is the vacuum permittivity and n (=4.15) is the refractive index of Si.

To analyze the thermal response of the tip under laser irradiation, a one-dimensional heat transfer model is used. As mentioned above, at the sharp end, the tip is a 500 nm conical apex with apex radius 10 nm and transitionally turns into a tetragonal pyramid base. In the heat transfer model, for simplicity, a 600 nm long conical with apex radius of 10 nm is connected to a tetragonal pyramid, and no transition is considered. Obviously, the thermal resistance for both ends should be computed separately with the same equation $\int dl/A_c k$, where A_c is the cross-section area, and k is local thermal conductivity; a schematic model of the tip is shown in Figure 9. The whole tip is divided into thin layers, each layer considered isothermal. For the tetragonal pyramid part, if the layer is irradiated by laser, the absorbed energy is $\alpha I A_s$, where A_s is the projection area exposed to laser, I is the incident laser intensity, and α is the absorption ratio. In the conical zone, due to small geometry, near-field heating is considered. The integration $\int_{conical} \beta I_{tip}\, dV$ represents the power absorbed by the tip, where I_{tip} can be expressed in term of electric field inside the tip E; the latter is calculated in the HFSS simulation. Considering the Poynting vector can be integrated over the surface of the conical tip in the HFSS model, and the net result of the integration is just the power absorbed by the tip, thus it is a convenient alternate. The temperature in the hemispherical apex is considered uniform in the heat transfer model.

The effects of small geometry and temperature on the thermal conductivity have been considered during our calculation. The thermal conductivity of the tip will be reduced due to its small geometry. Thermal transport is sustained by collisions among energy carries. In silicon, phonons are the dominant energy carriers, despite the presence of a certain amount of free charge heat carriers. The thermal conductivity in kinetic theory is given as

$$k = \frac{1}{3} C v l_{eff} \tag{2}$$

where C is the specific heat of the phonons, v is the average phonon speed, and l_{eff} is effective mean-free path, and is

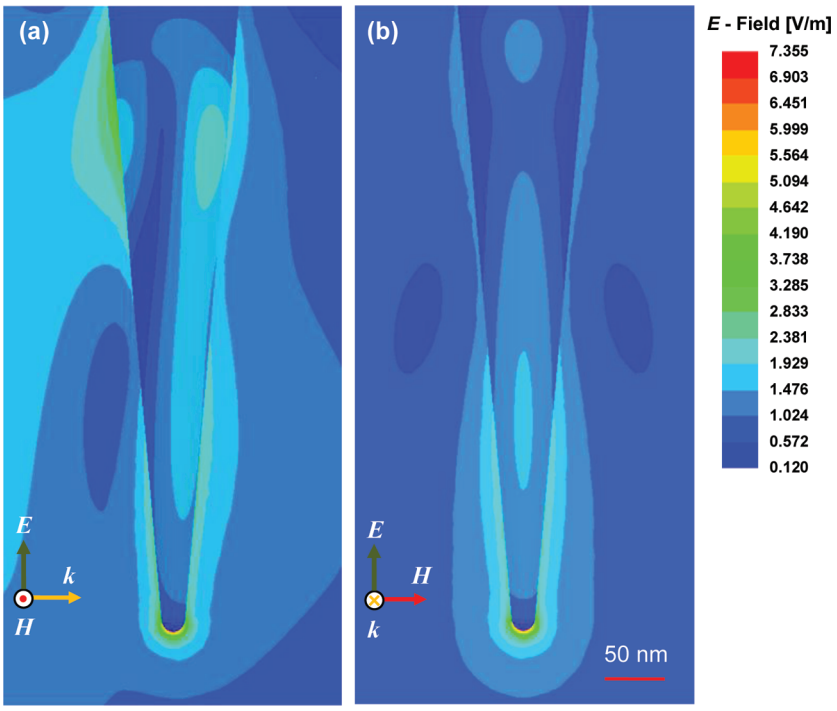

Figure 8. Field enhancement around the tip: (a) side view, (b) front view. The maximum electric field intensity is 2.14 V/m for the incident electric field intensity of 1 V/m. The electric field amplitude of the scattered light is equal to the field enhancement value, which is defined as the ratio of scattered to incident field amplitude.

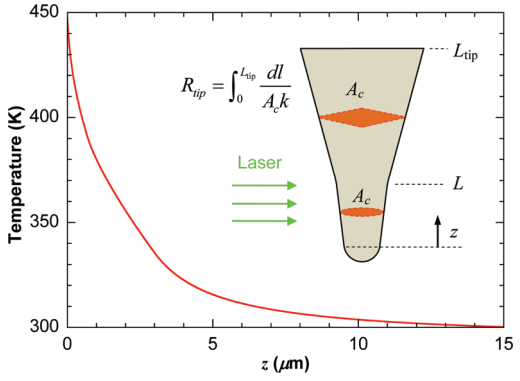

Figure 9. Steady-state temperature distribution along the tip axis. 2.8 μm at the tip apex is irradiated by laser with intensity of 5.6×10^8 W/m^2.

determined by[52]

$$\frac{1}{l_{\text{eff}}} = \frac{1}{\Lambda_\infty} + \frac{1}{d_c} \tag{3}$$

where Λ_∞ is the temperature-dependent phonon mean free path in bulk materials,[53] and d_c is the diameter of the structure; for the tip, d_c equals the diameter of the cross-section perpendicular to the tip axis. For simplicity, we choose $Cv = 1.68 \times 10^9$ W/m^2 K, neglecting the contribution of the optical phonons to the specific heat, because the optical phonons have little contribution to heat transfer.[53] Because the temperature-dependence on $k(T)$ is available for bulk Si,[54] as a result, the temperature-dependent phonon mean free path for bulk Si is $\Lambda_\infty(T) = 3k(T)/Cv$, when $d_c \rightarrow \infty$. Substitute $\Lambda_\infty(T)$ into eq 3, and then into eq 2, the temperature/geometry-dependent thermal conductivity of Si tip can be obtained.

The steady-state temperature distribution along the tip axis is shown in Figure 9. It shows that the temperature at the tip apex is 448 K. The measured temperature at the apex under 5.6×10^8 W/m^2 is ~600 K. Our first-order thermal analysis agrees well with the measurement results. The difference between them could be due to the tip geometry variation and reduction of Si tip thermal conductivity. The silicon tip is n-doped with antimony at a concentration ranging from 1 to 5×10^{18} ions/cm^3. The impurities and additional free carriers in doped silicon will reduce the thermal conductivity as compared to the value of pure bulk silicon[55] as well as in films[56−58] correspondingly. A reduction in thermal conductivity of 18% due to higher doping (1×10^{19} ions/cm^3, n- or p-type) was reported.[59] Therefore, the temperature acquired in the model is underestimated to some extent.

5. CONCLUSION

In this work, the temperature rise of Si AFM tip under laser irradiation was measured by using the Raman shift method with micrometer spatial resolution. The temperature was calibrated with an anharmonic model involving a three- and four-phonon process. Because of the small dimension of the laser spot and AFM tip, the focus will affect the result significantly during the experiment. Despite the fact that the interaction between tip and laser cannot be observed directly, the diffraction image of the tip under laser illumination can be used to monitor the focusing situation. It was found that the temperature could have strong distribution along the tip axis depending on the irradiation location of the laser spot. When the tip was moved upward closer to the focusing spot, the Raman shift decreased and the temperature increased; analogously, when the tip was moved upward away from the focusing spot, the Raman shift increased, and the temperature went down. Nevertheless, the Raman

intensity increased during the whole process. When the laser spot was moved along the tip axis from tip apex to cantilever, the temperature increased first, then decreased. The highest temperature was as high as 754 K. The incident laser intensity also strongly affected the heating condition. Under stronger laser irradiation, the Raman signal intensity was stronger, the Raman shift tends to be less, and the temperature went up. To investigate the mechanism of the near-field heating, the electric field distribution around the tip as well as inside the tip was calculated by using the finite element method. The highest field enhancement is 5.19 under the tip apex. Also, the highest field enhancement is 2.86 inside the tip. A one-dimensional heat transfer model was used to calculate the temperature distribution along the tip axis. The highest temperature was 448 K at the hemisphere apex, while the measured temperature was approximately 600 K. The difference between them could be induced by the further thermal conductivity reduction of the Si tip by its dopants, and underestimated laser scattering/absorption in the tip.

AUTHOR INFORMATION

Corresponding Author

*Tel.: (515) 294-2085. Fax: (515) 294-3261. E-mail: xwang3@iastate.edu.

ACKNOWLEDGMENT

X.C. thanks Yufeng Wu from ISU for taking SEM images of the AFM tip. Support of this work by the National Science Foundation (CMMI-0926704 and CBET-0932573) is gratefully acknowledged.

REFERENCES

(1) Kurpas, V. V.; Libenson, M. N.; Martsinovsky, G. A. Laser heat-up of near-field probe tip. *Proc. SPIE* **1995**, *2384*, 128–35.

(2) Kavaldjiev, D. I.; Toledo-Crow, R.; Vaez-Iravani, M. On the heating of the fiber tip in a near-field scanning optical microscope. *Appl. Phys. Lett.* **1995**, *67*, 2771–2773.

(3) La Rosa, A. H.; Yakobson, B. I.; Hallen, H. D. Origins and effects of thermal processes on near-field optical probes. *Appl. Phys. Lett.* **1995**, *67*, 2597–9.

(4) Lienau, C.; Richter, A.; Elsaesser, T. Light-induced expansion of fiber tips in near-field scanning optical microscopy. *Appl. Phys. Lett.* **1996**, *69*, 325–7.

(5) Stähelin, M.; Bopp, M. A.; Tarrach, G.; Meixner, A. J.; Zschokke-Gränacher, I. Temperature profile of fiber tips used in scanning near-field optical microscopy. *Appl. Phys. Lett.* **1996**, *68*, 2603–5.

(6) Downes, A.; Salter, D.; Elfick, A. Heating effects in tip-enhanced optical microscopy. *Opt. Express* **2006**, *14*, 5216–22.

(7) Chen, X.; Wang, X. Near-field thermal transport in a nanotip under laser irradiation. *Nanotechnology* **2011**, *22*, 075204−1–11.

(8) Zhang, W.; Schmid, T.; Yeo, B.-S.; Zenobi, R. Near-field heating, annealing, and signal loss in tip-enhanced Raman spectroscopy. *J. Phys. Chem. C* **2008**, *112*, 2104–8.

(9) Milner, A. A.; Zhang, K.; Garmider, V.; Prior, Y. Heating of an atomic force microscope tip by femtosecond laser pulses. *Appl. Phys. A: Mater. Sci. Process.* **2010**, *99*, 1–8.

(10) Chimmalgi, A. A.; Grigoropoulos, C. P.; Komvopoulos, K. Surface nanostructuring by nano-/femtosecond laser-assisted scanning force microscopy. *J. Appl. Phys.* **2005**, *97*, 104319-1–12.

(11) Mai, Z. H.; Lu, Y. F.; Song, W. D.; Chim, W. K. Nano-modification on hydrogen-passivated Si surfaces by a laser-assisted scanning tunneling microscope operating in air. *Appl. Surf. Sci.* **2000**, *154−155*, 360–4.

(12) Mamin, H. J.; Rugar, D. Thermomechanical writing with an atomic force microscope tip. *Appl. Phys. Lett.* **1992**, *61*, 1003–1005.

(13) McCarthy, B.; Zhao, Y.; Grover, R.; Sarid, D. Enhanced Raman scattering for temperature measurement of a laser-heated atomic force microscope tip. *Appl. Phys. Lett.* **2005**, *86*, 111914−1–3.

(14) Hamann, H. F.; Martin, Y. C.; Wickramasinghe, H. K. Thermally assisted recording beyond traditional limits. *Appl. Phys. Lett.* **2004**, *84*, 810–2.

(15) Huber, R.; Koch, M.; Feldmann, J. Laser-induced thermal expansion of a scanning tunneling microscope tip measured with an atomic force microscope cantilever. *Appl. Phys. Lett.* **1998**, *73*, 2521–3.

(16) Boneberg, J.; Münzer, H.-J.; Tresp, M.; Ochmann, M.; Leiderer, P. The mechanism of nanostructuring upon nanosecond laser irradiation of a STM tip. *Appl. Phys. A: Mater. Sci. Process.* **1998**, *67*, 381–4.

(17) Tarun, A.; Hayazawa, N.; Kawata, S. Site-selective cutting of carbon nanotubes by laser heated silicon tip. *Jpn. J. Appl. Phys.* **2010**, *49*, 025003-1–4.

(18) Nelson, B.; King, W. Modeling and simulation of the interface temperature between a heated silicon tip and a substrate. *Nanoscale Microscale Thermophys. Eng.* **2008**, *12*, 98–115.

(19) Duvigneau, J.; Schönherr, H.; Vancso, G. J. Nanoscale thermal AFM of polymers: transient heat flow effects. *ACS Nano* **2010**, *4*, 6932–40.

(20) Geshev, P. I.; Demming, F.; Jersch, J.; Dickmann, K. Calculation of the temperature distribution on laser-illuminated scanning probe tips. *Appl. Phys. B: Laser Opt.* **2000**, *70*, 91–7.

(21) Geshev, P. I.; Klein, S.; Dickmann, K. Calculation of the temperature and thermal expansion of a STM tip heated by a short laser pulse. *Appl. Phys. B: Laser Opt.* **2003**, *76*, 313–7.

(22) Grafström, S.; Kowalski, J.; Numann, R; Probst, O.; Wörtge, M. Analysis and compensation of thermal effects in laser-assisted scanning tunneling microscopy. *J. Vac. Sci. Technol., B* **1991**, *9*, 568–72.

(23) Grafström, S.; Schuller, P.; Kowalski, J.; Neumann, R. Thermal expansion of scanning tunneling microscopy tips under laser illumination. *J. Appl. Phys.* **1998**, *83*, 3453–60.

(24) Jersch, J.; Demming, F.; Fedotov, I.; Dickmann, K. Time-resolved current response of a nanosecond laser pulse illuminated STM tip. *Appl. Phys. A: Mater. Sci. Process.* **1999**, *68*, 637–41.

(25) Lyubinetsky, I.; Dohnálek, Z.; Ukraintsev, V. a.; Yates, J. T. Transient tunneling current in laser-assisted scanning tunneling microscopy. *J. Appl. Phys.* **1997**, *82*, 4115–7.

(26) Novotny, L.; Bian, R. X.; Xie, X. S. Theory of nanometric optical tweezers. *Phys. Rev. Lett.* **1997**, *79*, 645–8.

(27) Yue, Y.; Chen, X.; Wang, X. Noncontact sub-10 nm temperature measurement in near-field laser heating. *ACS Nano* **2011**, *5*, 4466–4475.

(28) Hsu, I.-K.; et al. Optical measurement of thermal transport in suspended carbon nanotubes. *Appl. Phys. Lett.* **2008**, *92*, 063119-1–3.

(29) Yue, Y.; Eres, G.; Wang, X.; Guo, L. Characterization of thermal transport in micro/nanoscale wires by steady-state electro-Raman-thermal technique. *Appl. Phys. A: Mater. Sci. Process.* **2009**, *97*, 19–23.

(30) Ioffe, Z.; et al. Detection of heating in current-carrying molecular junctions by Raman scattering. *Nat. Nanotechnol.* **2008**, *3*, 727–32.

(31) Soini, M.; et al. Thermal conductivity of GaAs nanowires studied by micro-Raman spectroscopy combined with laser heating. *Appl. Phys. Lett.* **2010**, *97*, 263107−1–3.

(32) Piscanec, S.; et al. Raman spectroscopy of silicon nanowires. *Phys. Rev. B* **2003**, *68*, 241312−1–4.

(33) Su, Z.; et al. Temperature-dependent Raman scattering of silicon nanowires. *J. Phys. Chem. B* **2006**, *110*, 1229–34.

(34) Khachadorian, S.; Scheel, H.; Colli, A.; Vierck, A.; Thomsen, C. Temperature dependence of first- and second-order Raman scattering in silicon nanowires. *Phys. Status Solidi B* **2010**, *247*, 3084–8.

(35) Niu, J.; Sha, J.; Yang, D. Temperature dependence of the first-order Raman scattering in silicon nanowires. *Scr. Mater.* **2006**, *55*, 183–186.

(36) Konstantinović, M.; et al. Raman scattering in cluster-deposited nanogranular silicon films. *Phys. Rev. B* **2002**, *66*, 161311−1–4.

(37) Hart, T. R.; Aggarwal, R. L.; Lax, B. Temeprature dependence of Raman scattering in silicon. *Phys. Rev. B* **1970**, *1*, 638–42.
(38) Zhang, S.-L.; et al. Variation of Raman feature on excitation wavelength in silicon nanowires. *Appl. Phys. Lett.* **2002**, *81*, 4446–8.
(39) Balkanski, M.; Wallis, R. F.; Haro, E. Anharmonic effects in light scattering due to optical phonons in silicon. *Phys. Rev. B* **1983**, *28*, 1928–34.
(40) Tsu, R. Temperature dependence of silicon Raman lines. *Appl. Phys. Lett.* **1982**, *41*, 1016–8.
(41) Doerk, G.; Carraro, C.; Maboudian, R. Temperature dependence of Raman spectra for individual silicon nanowires. *Phys. Rev. B* **2009**, *80*, 1–4.
(42) Serrano, J. R.; Phinney, L. M.; Kearney, S. P. Micro-Raman thermometry of thermal flexure actuators. *J. Micromech. Microeng.* **2006**, *16*, 1128–34.
(43) Abel, M. R.; Graham, S.; Serrano, J. R.; Kearney, S. P.; Phinney, L. M. Raman thermometry of polysilicon microelectro-mechanical systems in the presence of an evolving stress. *J. Heat Transfer* **2007**, *129*, 329–34.
(44) Menendez, J.; Cardona, M.; Festkorperforschung, M. P. Temperature dependence of the first-order Raman scattering by phonos in Si, Ge, and a-Sn: Anharmonic effects. *Phys. Rev. B* **1984**, *29*, 2051–9.
(45) Gerstner, V.; Thon, A.; Pfeiffer, W. Thermal effects in pulsed laser assisted scanning tunneling microscopy. *J. Appl. Phys.* **2000**, *87*, 2574–80.
(46) Jin, J. M. *The Finite Element Method in Electromagnetics*; Wiley-IEEE Press: New York, 2002.
(47) Micic, M.; Klymyshyn, N.; Suh, Y. D.; Lu, H. P. Finite element method simulation of the field distribution for AFM tip-enhanced surface-enhanced Raman scanning microscopy. *J. Phys. Chem. B* **2003**, *107*, 1574–84.
(48) Shi, J.; et al. Laser-assisted nanoscale deposition of diamond-like carbon films on tungsten tips. *Appl. Phys. Lett.* **2004**, *85*, 1009–11.
(49) Royer, P.; Barchiesi, D.; Lerondel, G.; Bachelot, R. Near-field optical patterning and structuring based on local-field enhancement at the extremity of a metal tip. *Philos. Trans. R. Soc., A* **2004**, *362*, 821–42.
(50) Downes, A.; Salter, D.; Elfick, A. Finite element simulations of tip-enhanced Raman and fluorescence spectroscopy. *J. Phys. Chem. B* **2006**, *110*, 6692–8.
(51) Zhang, W.; Cui, X.; Martin, O. J. F. Local field enhancement of an infinite conical metal tip illuminated by a focused beam. *J. Raman Spectrosc.* **2009**, *40*, 1338–42.
(52) Ju, Y. S. Phonon heat transport in silicon nanostructures. *Appl. Phys. Lett.* **2005**, *87*, 153106-1–3.
(53) Chen, G. Thermal conductivity and ballistic-phonon transport in the cross-plane direction of superlattices. *Phys. Rev. B* **1998**, *57*, 14958–73.
(54) Incropera, F. P.; Dewitt, D. P.; Bergman, T. L.; Lavine, A. S. *Fundamentals of Heat and Mass Transfer*; John Wiley & Sons: New York, 2006; p 931.
(55) Goodson, K. E.; Cooper, P. T. The effect of high-energy electrons on lattice conduction in semiconductor devices. *Proc. Symp. Thermal Sci. Eng. Honor Chancellor Chang-Lin Tien* **1995**, 153–9.
(56) Asheghi, M.; Touzelbaev, M. N.; Goodson, K. E.; Leung, Y. K.; Wong, S. S. Temperature-dependent thermal conductivity of single-crystal silicon layers in SOI substrates. *J. Heat Transfer* **1998**, *120*, 30–6.
(57) Asheghi, M.; Kurabayashi, K.; Kasnavi, R.; Goodson, K. E. Thermal conduction in doped single-crystal silicon films. *J. Appl. Phys.* **2002**, *91*, 5079–88.
(58) Liu, W.; Asheghi, M. Thermal conduction in ultrathin pure and doped single-crystal silicon layers at high temperatures. *J. Appl. Phys.* **2005**, *98*, 123523−1–6.
(59) Burzo, M. G.; Komarov, P. L.; Raad, P. E. Non-contact thermal conductivity measurements of p-doped and n-doped gold covered natural and isotopically-pure silicon and their oxides. *5th Intl. Conf. on Thermal and Mechanical Simulation and Experiments in Microelectronics and Microsystems (EuroSimE 2004)*, 2004; pp 269−76, doi: 10.1109/ESIME.2004.1304050.
(60) Burke, H. H.; Herman, I. P. Temperature dependence of Raman scattering in Ge1−xSix alloys. *Phys. Rev. B* **1993**, *48*, 16–24.